MATERIALS AND COMPONENT DEVELOPMENT FOR ADVANCED TURBINE SYSTEMS

M. A. Alvin
National Energy Technology Laboratory
626 Cochrans Mill Road
Pittsburgh, PA 15236-0940

F. Pettit, G. Meier, N. Yanar, M. Chyu, D. Mazzotta, W. Slaughter, V. Karaivanov
Mechanical Engineering and Material Science
University of Pittsburgh
Pittsburgh, PA 15260

B. Kang, C. Feng, R. Chen, T-C. Fu
Mechanical and Aerospace Engineering & Civil Engineering
West Virginia University
Morgantown, WV 26506

Abstract

In order to meet the 2010-2020 DOE Fossil Energy goals for Advanced Power Systems, future oxy-fuel and hydrogen-fired turbines will need to be operated at higher temperatures for extended periods of time, in environments that contain substantially higher moisture concentrations in comparison to current commercial natural gas-fired turbines. Development of modified or advanced material systems, combined with aerothermal concepts are currently being addressed in order to achieve successful operation of these land-based engines.

To support the advanced turbine technology development, the National Energy Technology Laboratory (NETL) has initiated a research program effort in collaboration with the University of Pittsburgh (UPitt), and West Virginia University (WVU), working in conjunction with commercial material and coating suppliers as Howmet International and Coatings for Industry (CFI), and test facilities as Westinghouse Plasma Corporation (WPC) and Praxair, to develop advanced material and aerothermal technologies for use in future oxy-fuel and hydrogen-fired turbine applications. Our program efforts and recent results are presented.

Introduction

Increasing the power efficiency of stationary land-based industrial gas turbines will require future turbine inlet temperatures to increase to >1400°C (Table 1). Cooling air will simultaneously need to be controlled to avoid an increase in NO_x emissions. The concept of

ultra low or “zero” emission power generation has focused on an oxy-fuel combustion process in which nitrogen is removed in the combustion air, and replaced with steam, thereby preventing the formation of nitrogen oxides. The exhaust stream of the oxy-fuel process is separated into concentrated CO_2 and water.

The development of oxy-fuel gas turbine IGCC plants has two major benefits: (1) the turbine exhaust gas is a highly enriched CO_2 stream with a small amount of excess oxygen. This exhaust gas can be processed to reduce excess oxygen to satisfy sequestration oxygen requirements if needed, then dried and compressed, reducing the cost and plant performance impact of CO_2 removal for sequestration compared to the standard IGCC plant configuration; (2) the syngas, recycle CO_2, and oxygen streams fed to the oxy-fuel turbine combustors will contain very little nitrogen. Thus, NO_x emissions from the gas turbine will be very low, eliminating the need for expensive, low-NO_x combustors and SCR exhaust gas NO_x reduction.

Alternately, hydrogen-fueled combustion turbine systems are conceptually based on a complex cycle composed of a closed Brayton and Rankine cycle. Hydrogen turbines are expected to be a key part of near-term integrated gasification combined cycle (IGCC) plants that can sequester carbon dioxide, such as FutureGen. Hydrogen and oxygen are supplied as the fuel and oxidant respectively to a compressor, and burned in steam. The pressurized steam feed enters a high temperature turbine at 1700°C for stator blades, and 1570°C for rotor blades. Since these elevated temperatures are typically higher than the melting temperatures of alloys used in the construction of the hot gas structural components, the components are cooled by air extracted from the turbine compressor and directed through the cooling passages designed into the component.

Oxidation and hot corrosion in commercial land-based power generation gas turbines are principal concerns, particularly in view of long-term operation (30,000 hrs), as well operation with advanced combustion cycles that potentially target turbine inlet temperatures of >1500°C. Current structural materials as nickel and cobalt-based superalloys cannot withstand temperatures of >950°C. Although single crystal substrates as René N5, CMSX-4, PM2000, and the like, increase the durable operating temperature for the structural airfoil support, operation in the advanced combustion cycles will require development and application of stable thermal barrier coatings (TBCs) with better insulation properties, as well as implementation of acceptable internal component cooling techniques, in order to achieve extended operational life of oxy-fuel and hydrogen fired land-based turbines.

Bond Coat Development and Assessment

As a candidate alloy for advanced turbine blades, the single crystal René N5 matrix was selected in this program for its high temperature creep resistant characteristics, and oxidative stability which results from the formation of a protective external alumina scale. As a combustor liner or disc matrix, the nickel-based superalloy, Haynes 230, was also selected in this program for its high temperature oxidative stability, but primarily for its ability to form an external protective

chromia scale. By addressing the response of both metal substrates and their TBC counterparts, information is being generated that potentially could support the use of either alloy at alternate turbine component design locations.

In conjunction with CFI, NETL initiated development of a bond coat system that consisted of metallic-ceramic particles that were held together via an inorganic binder. When applied to René N5 and Haynes 230 coupons manufactured at Howmet International, preliminary bench-scale testing at CFI indicated adherence of the porous ~40-50 μm thick NETL-1 bond coat after being subjected to (1) 24 hrs of static air exposure at 800°C; (2) 10 severe thermal cycles (100°C/minute ramp rate from room temperature to 1000°C, followed by 1 hr dwell time at temperature, then rapid cooling); and 3) 500 hrs of static air testing at 1000°C.

Extended thermal cycle testing was then conducted at 900°C and 1100°C under static conditions for 2,000 hrs. Although the initial NETL-bond coat remained adherent to the base metal substrates at 900°C, the coupons experienced a weight increase indicative of the oxidation throughout the bond coat, as well as along the René N5 and Haynes 230 substrate interfaces. At 1100°C, weight loss of the coupons was observed after 200 hrs, which reflected localized spalling of the coating during both thermal cycling and isothermal testing. Oxidation along the single crystal and superalloy substrate interface was also observed. Similar results were demonstrated when thermal cycling was conducted in the presence of water vapor.

To improve adherence of the bond coat at 1100°C and mitigate oxygen permeation, modifications to the NETL-CFI bond coat were made, subsequently leading to production of a densified metallic coating (Figure 1). Currently extended thermal cycle testing is being conducted to demonstrate the performance of the modified NETL-A1 architecture at 900°C and 1100°C. The rationale for testing at 1100°C is to screen potential alternate bond coat systems, comparing their performance to that of state-of-the-art (SOTA) materials, prior to addressing performance at the advanced turbine operating temperatures shown in Table 1.

Testing has also been initiated at the Westinghouse Plasma Corporation (WPC) facility where rotating (500 rpm), NETL-A1-coated, René N5 tubes are being subjected to external surface temperatures of 1100°C, while being internally cooled with air (Figure 2). After extended exposure (i.e., ~500 hrs), post-test analysis of the tubes will include visual inspection, and measurements to determine thinning of the outer coating. Due to the material and fabrication cost for each tube, post-test destructive characterization will not be performed. Non-destructive evaluation (NDE) techniques, as described in the following section, are planned. Demonstration of the stability and performance of material systems when subjected to an applied heat flux at WPC serves as the basis for extended screening of potential material systems for use in advanced turbine applications, and is being conducted in conjunction with our aerothermal efforts which are also described in this paper.

Efforts have also been focused on the application and adherence of an air plasma sprayed (APS) and electron beam physical vapor deposited (EBPVD), yttria stabilized zirconia (YSZ), top coat along the outer surface of NETL bond coat systems. As shown in Table 2, early failure resulted

for the original NETL-1 bond coat system when either the APS or EBPVD YSZ architecture had been subjected to 1100°C thermal cycle testing. Debonding along the metal substrate interface was principally attributed to the adhesion characteristics of the porous as-manufactured NETL-1 bond coat. The surface roughness of the bond coat also lead to irregular columnar growth of the EBPVD YSZ layer (Figure 3). For state-of-the-art CoNiCrAlY-YSZ systems (Figure 4), cycle time-to-failure during 1100°C cyclic oxidation testing was extended. The absence of an applied bond coat system was shown to further promote retention of the YSZ top coat along the surface of the base metal substrates. Extended cycle time-to-failure was observed for APS YSZ on the René N5, an alumina former, while the longest cycle time-to-failure identified to date was EBPVD YSZ on Haynes 230, a chromia former.

Material Diagnostics

Micro-Indentation Testing — Surface Stiffness Response

Recent efforts have been focused on development of a simplified micro-indentation technique (MIT) for monitoring changes in the mechanical properties of bond coat and TBC systems, and ultimately addressing their integrity and life during extended process operation. The MIT consists of a 1.6 mm diameter spherical indenter assembly that is attached to a load cell, which is in turn attached to a PZT actuator. The PZT actuator provides the overall indentation depth measurement which includes the indentation penetration depth and system rigid-body displacement.

Initially, the contact position between the indenter and the surface of the sample is determined for a given load threshold (i.e., 0.1-5N). Subsequently multi-loading and partial-unloading indentation tests are conducted using pre-defined parameters as velocity of the indenter, the penetration depth (i.e., ~10 μm), and the unloading compliance. From the multiple unloading compliance measurements, the effect of system rigid-body displacement is eliminated, and true surface stiffness response of the bond-coated coupons is then determined. Using this technique on flat, polished, 25mm x 25mm x 3mm coupons, a Young's modulus of ~200-210 GPa was determined for Haynes 230, which is in good agreement with literature reported values. The Young's modulus for the single crystal René N5 matrix was identified as ~130-150 GPa. In contrast to defining Young's modulus, an overall surface stiffness response of the coating/substrate architecture was determined due to the irregular morphology of the bond coat surface (1).

When bond-coated René N5 and Haynes 230 coupons were subjected to thermal cycling conditions (25° ↔ 1100°C), the overall surface stiffness response of the coating was shown to decrease with continued cycling (Figure 5). These results strongly correlate with weight change measurements of the coupons after completion of the 100, 200, 300, and 400 thermal cycles. In addition, the greater calculated loss of bond coat stiffness on the Haynes 230 matrix reflected the greater extent of surface crack formations and areas of spallation in comparison to that which resulted along the surface of the thermally cycled, bond-coated, René N5 coupons.

Acousto-Ultrasonics

A nonlinear acousto-ultrasonic technique is also being developed to evaluate interface delamination of bond coatings that are applied to the surface of single crystal and superalloy metal substrates. A greater nonlinear response in the waveform amplitude-dependent characteristics is projected to result when debonding or delamination of the bond coat and/or top coat layers occurs.

The bench-scale test equipment consists of a laser vibrometer and a spectrum analyzer with various ultrasonic transducers, and digitization/acquisition boards that can detect kHz-MHz frequencies. Due to the size of coupons (25mm x 25mm x 3mm), miniature piezoelectric sensors were used. In order to assure that the distance between the pulser and receiver was fixed, both sensors were attached to an acrylic block which served as a sensor bridge. A stretched latex membrane was used as the dry contact interface between the sensor and the coupon surface. A constant sensor contact pressure of 0.6 MPa was applied to the coupon surface, and a series of 30 readings were generated typically along the center of the coupon to assure statistical accuracy of the resulting data.

Testing was performed on (1) uncoated base metal coupons; (2) as-manufactured coated coupons; and (3) coated coupons that had been subjected to 100, 200, 300, and 400 thermal cycles (25° to 1100°C). A wave propagation analysis was conducted using Lamb's solution for an axisymmetric analysis of an elastic half-space due to a point load at the origin. Although the ultrasonic waveform was virtually the same for the bond-coated René N5 coupon after being subjected to 100, 200, 300, and 400, 1100°C thermal cycles, slight shifting in travel time was observed (Figure 6). This implied that material properties as Young's modulus, density, or other geometry changes had occurred. In contrast, marked differences in the waveform and travel time were observed for the bond-coated Haynes 230 coupon. Discontinuity or localized debonding and/or delamination of the coating from the surface of the Haynes 230 matrix was expected to have occurred. Notably, repeatability of the wave characteristics was observed for the thermal-cycled René N5 matrix, implying more overall uniformity and consistency of the residual bond coat.

In conjunction with experimental testing, a finite element method (FEM) for wave propagation simulation was conducted using ABAQUS. Material properties were assumed to be E = 211 GPa and ρ = 8,970 kg/m^3 for Haynes 230, and E = 213 GPa and ρ = 8,630 kg/m^3 for René N5 base metal substrates. FEM time histories of the surface vertical waveform displacement were shown to be comparable to the theoretical solutions for both the arrival time and peak amplitude. In contrast for bond-coated systems, the peak amplitudes and their corresponding arrival times were seen to be clearly influenced by assumed material properties (Figure 7). Similarly when embedded voids were included in modulated sine impulse FEM simulations to reflect delamination of the coating, a strong nonlinear effect from the void with higher harmonics resulted (Figure 8). Correlation of the FEM delamination simulation data with the experimentally generated results for the 100-400 thermally cycled coupons is being undertaken.

Aerothermal-Materials Integration

A computational methodology based on three-dimensional numerical simulation and damage mechanics for predicting thermal-mechanical durability and life of turbine blades is being developed for hydrogen-fired and oxy-fuel applications. Efforts have focused on analysis of stress distributions due to temperature, pressure, and centrifugal loads for a solid NASA E^3 blade model (Figure 9) (2). To complete the thermal-mechanical analysis of the solid substrate, the level of thermal load or boundary condition on the airfoil external surface was determined via 3D CFD simulation modeling using FLUENT. While the heat transfer coefficient was shown to vary strongly along the surface of the airfoil, the projected trends were relatively comparable for airfoils in syngas and hydrogen-fired applications (Table 1). Modeling projected the highest surface temperatures along the leading edge of single crystal airfoils (i.e., CSMX-4; René N5), as well as airfoils with an applied MCrAlY-YSZ TBC (Figure 10). When combined thermal, surface pressure, and centrifugal loads were applied to the model airfoil, the highest stress resulted along the mid-rib and near the root section of the blade (Figure 11).

Currently efforts are being directed to incorporate the finite element analysis (FEA) results into a life prediction model that is capable of evaluating creep evolution damage over the entire airfoil, as well as visualizing the results of the life prediction analysis, and identifying the most critical zones (3). Recent creep damage calculations with a mechanical load comparable to that of future hydrogen-fired systems identified significant short-term impact again along the blade's leading edge, mid-rib, and near the base of the trailing edge (Figure 12). Reducing temperature by 30% over the entire blade projected a significant increase in service operating life (Figure 13).

Acknowledgments

We wish to acknowledge Mr. Richard Dennis, DOE NETL Turbine Technology Manager, for his continued support of this project. The efforts of Mr. James Klotz at CFI, Mr. Bob Grunstra, Mr. Ty Hansen, Mr. Ron Honick, and Mr. Ken Murphy at Howmet International, and Dr. Shyam Dighe and Dr. Ivan Martorell at WPC are gratefully acknowledged.

References

1. C. Feng, M.A. Alvin, B.S.-J. Kang, "A Micro-Indentation Method for Assessment of TBC Bond Coat Systems," Paper No. 351171, presented at the MS&T 2007 Conference, Detroit, MI (September 2007).

2. D. Mazzotta, M.K. Chyu, M.A. Alvin, "Aero-Thermal Characterization of Hydrogen Turbines," Paper No. GT2007-28296, presented at the ASME Turbo Expo 2007, Land, Sea and Air Conference, Montreal, Canada (May 2007).

3. V. Karaivanov, D. Mazzotta, W. Slaughter, M. Chyu, M.A. Alvin, "Three-dimensional Modeling of Creep Damage in Airfoils for Advanced Turbine Systems," Paper No. GT2008-

51278 to be presented at the ASME Turbo Expo 2008, Gas Turbine Technical Congress and Exposition, Berlin, Germany (June 2008).

Table 1: Advanced Turbine Operating Conditions

	Syngas Turbine 2010	Hydrogen Turbine 2015-2020	Oxy-Fuel Turbine 2010	Oxy-Fuel Turbine 2015-2020
Combustor Exhaust Temp, °F (°C)	~+2700 (~+1480)	~+2700 (~+1480)		
Turbine Inlet Temp, °F (°C)	~2500 (~1370)	~2600 (~1425)	~1150 (~620)	~1400 (~760) (HP) ~3200 (~1760) (IP)
Turbine Exhaust Temp, °F (°C)	~1100 (~595)	~1100 (~595)		
Turbine Inlet Pressure, psig	~265	~300	~450	~1500 (HP) ~625 (IP)
Combustor Exhaust Composition	9.27% CO_2 8.5% H_2O 72.8% N_2 0.8% Ar 8.6% O_2	1.4% CO_2 17.3% H_2O 72.2% N_2 0.9% Ar 8.2% O_2	82% H_2O 17% CO_2 0.1% O_2 1.1% N_2 1% Ar	75-90% H_2O 25-10% CO_2 1.7% O_2, N_2, Ar

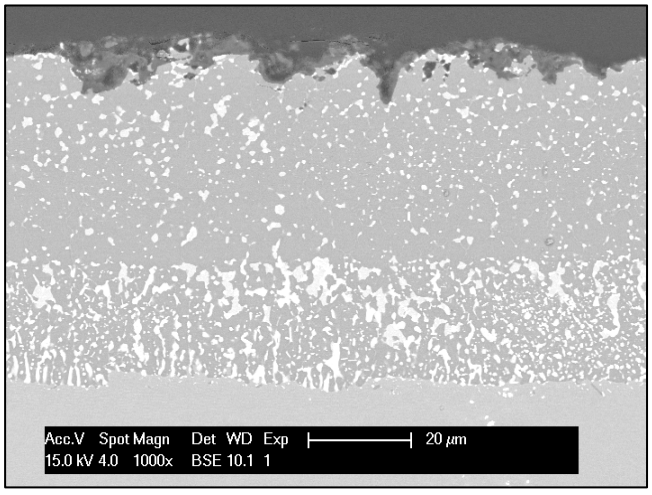

Figure 1. NETL-A1 Bond Coat System

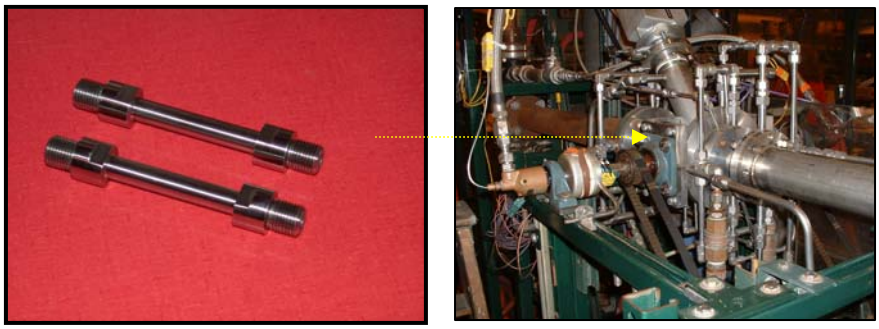

Figure 2. Bond-Coated René N5 Tubes Used for Thermal Flux Testing at the Westinghouse Plasma Corporation Test Facility

Table 2: Cyclic Oxidation Testing of NETL and SOTA TBC Systems at 1100°C
— Cycles to Failure —

Bond Coat + YSZ Top Coat	Substrate	
	René N5	Haynes 230
NETL-1 + APS	20	20
NETL-1 + EBPVD	40	120-140
NETL-A1 + APS		
NETL-A1 + EBPVD		
MCrAlY + APS	200	220-240
MCrAlY + EBPVD		
Pt-Al + EBPVD		
– + APS	240	60
– + EBPVD	320-400	460-480

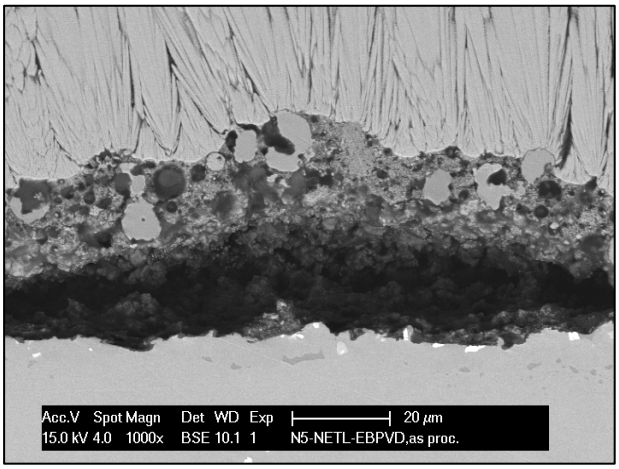

Figure 3. EBPVD YSZ on the NETL-1 Bond Coat

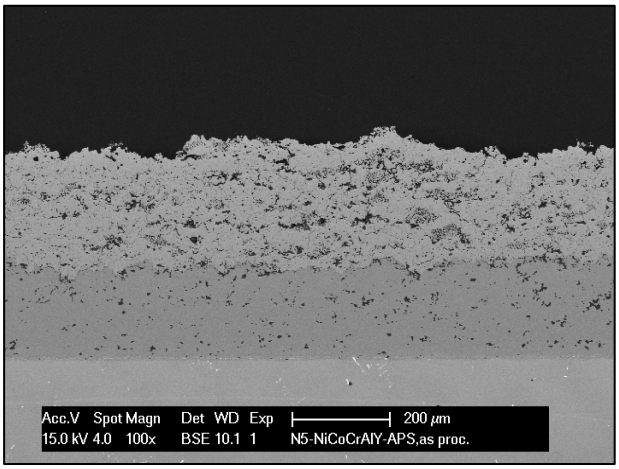

Figure 4. APS YSZ on a CoNiCrAlY Bond Coat

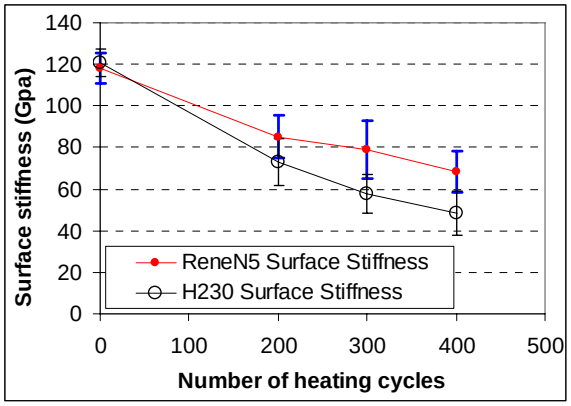

Figure 5. Bond Coat Stiffness Comparison on René N5 and Haynes 230 Alloy as a Function of Extended, High Temperature, Cyclic Oxidation

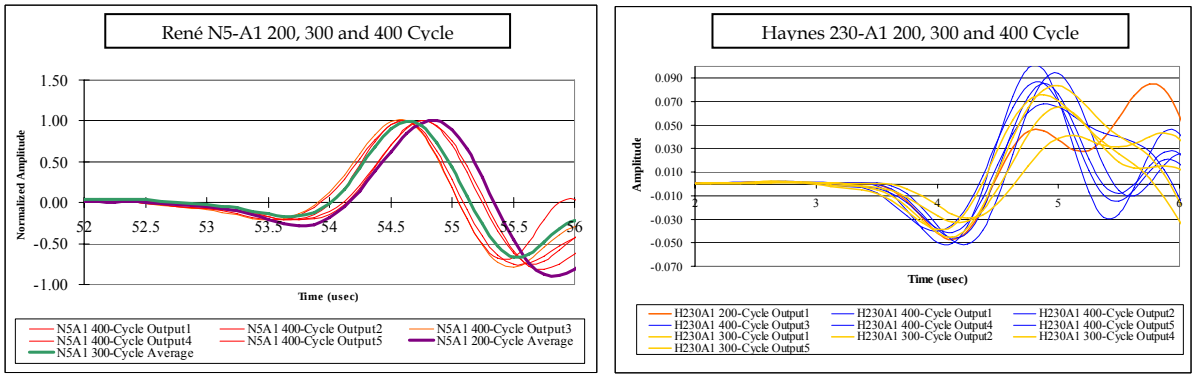

Figure 6. Wavefronts for Bond-Coated René N5 and Haynes 230 Coupons after Exposure to 100-400 Thermal Cycles

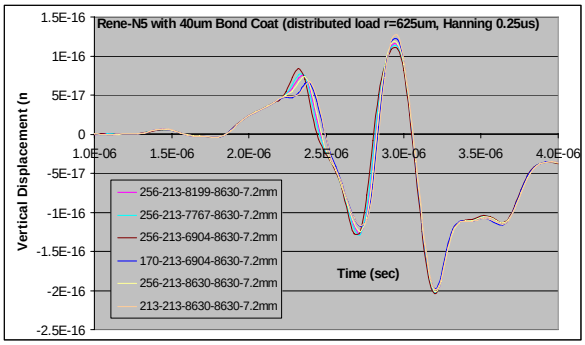

Figure 7. Influence of Bond Coat Properties on Surface Displacement Time History

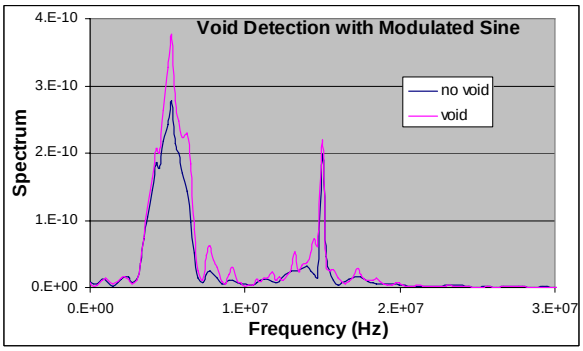

Figure 8. Spectrum of Delaminated TBCs with Modulated Sine Excitations

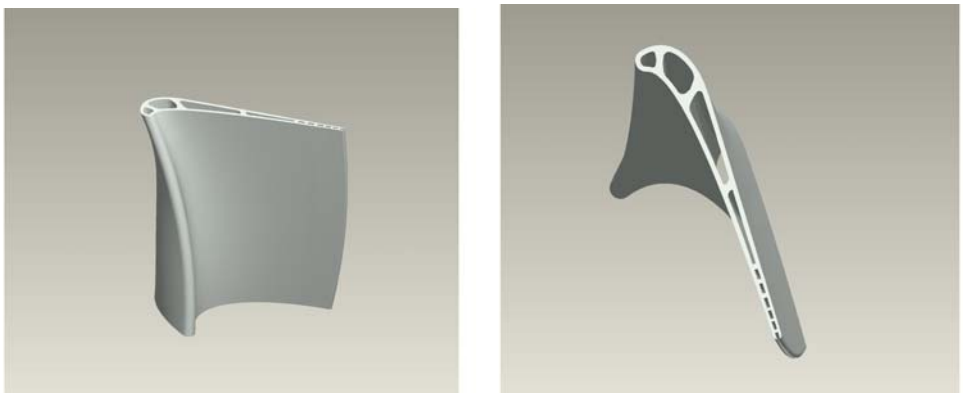

Figure 9. Solid Model of the NASA E^3 Blade, Created Using Pro/Engineer and the Finite Element Analysis Application ANSYS

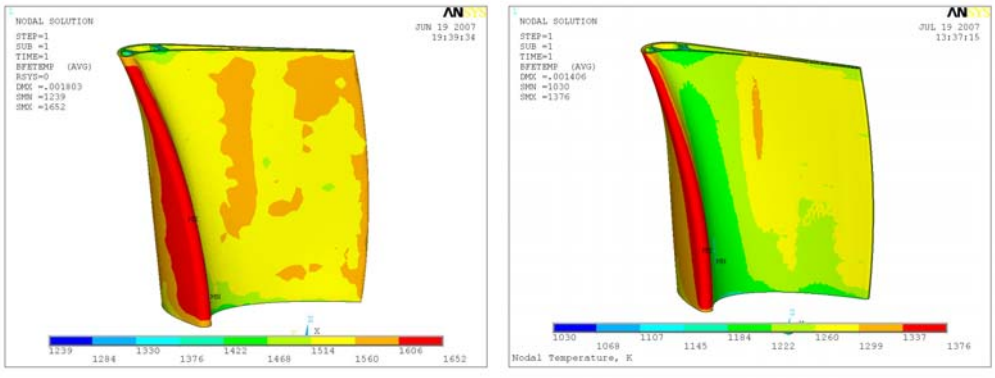

Figure 10. Base Metal and External TBC Surface Contour Temperature Distribution Plots, in Kelvin, for Hydrogen-Fired Airfoil Applications

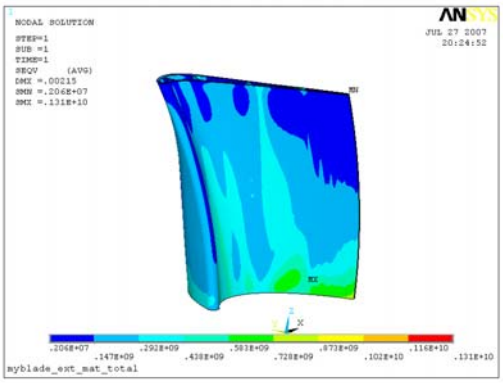

Figure 11. Stress Distribution Plot, in Pascals, Resulting from the Combined Thermal, Surface Pressure, and Centrifugal Loads (Applied Angular Velocity of 15,000 rpm; Rotor Radius of 0.35 m)

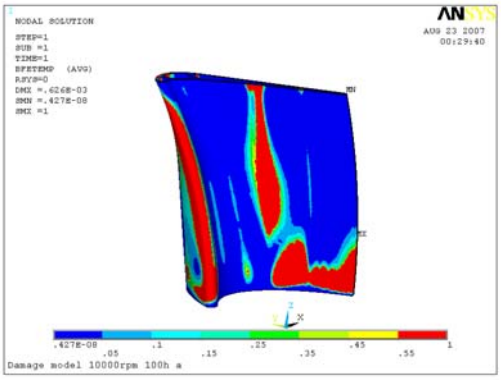

Figure 12. Creep Damage: 100 hrs, 10k rpm

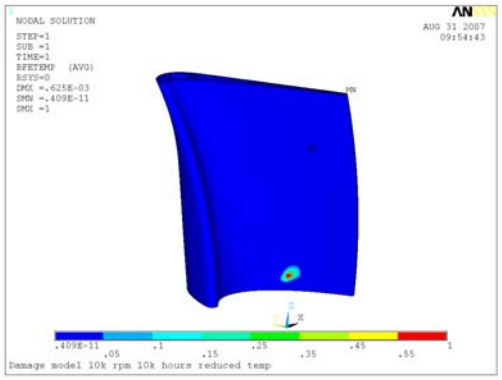

Figure 13. Creep Damage: 10,000 hrs, 10k rpm, Reduced Thermal Load